

Article

Optimal Sizing of Battery and Super-Capacitor Based on the MOPSO Technique via a New FC-HEV Application

Abdeldjalil Djouahi ^{1,*}, Belkhir Negrou ¹, Boubakeur Rouabah ², Abdelbasset Mahboub ²
and Mohamed Mahmoud Samy ³

¹ Laboratory Promotion et Valorisation des Ressources Sahariennes (VPRS), University of Kasdi Merbah Ouargla, BP 511, Ouargla 30000, Algeria

² Electrical Engineering Department, University of Kasdi Merbah Ouargla, BP 511, Ouargla 30000, Algeria

³ Electrical Engineering Department, Faculty of Engineering, Beni-Suef University, Beni-Suef 2722165, Egypt

* Correspondence: djouahi1994@gmail.com

Abstract: In light of the energy and environment issues, fuel cell vehicles have many advantages, including high efficiency, low-temperature operation, and zero greenhouse gas emissions, making them an excellent choice for urban environments where air pollution is a significant problem. The dynamics of fuel cells, on the other hand, are relatively slow, owing principally to the dynamics of the air compressor and the dynamics of manifold filling. Because these dynamics can limit the overall performance of fuel cell vehicles, two key technologies that have emerged as critical components of electric vehicle powertrains are batteries and supercapacitors. However, choosing the best hybrid energy storage system that combines a battery and a supercapacitor is a critical task nowadays. An electric vehicle simulated application by MATLAB Code is modeled in this article using the multi-objective particle swarm optimization technique (MOPSO) to determine the appropriate type of batteries and supercapacitors in the SFTP-SC03 drive cycle. This application optimized both component sizing and power management at the same time. Batteries of five distinct types (Lithium, Li-ion, Li-S, Ni-NiCl₂, and Ni-MH) and supercapacitors of two different types (Maxwell BCAP0003 and ESHSR-3000CO) were used. Each storage component is distinguished by its weight, capacity, and cost. As a consequence, using a Li-ion battery with the Maxwell BCAP0003 represented the optimal form of hybrid storage in our driving conditions, reducing fuel consumption by approximately 0.43% when compared to the ESHSR-3000CO.

Keywords: fuel-cell hybrid electric vehicle; particle swarm optimization algorithm; hydrogen consumption; multi-objective function problem; energy management strategy



Citation: Djouahi, A.; Negrou, B.; Rouabah, B.; Mahboub, A.; Samy, M.M. Optimal Sizing of Battery and Super-Capacitor Based on the MOPSO Technique via a New FC-HEV Application. *Energies* **2023**, *16*, 3902. <https://doi.org/10.3390/en16093902>

Academic Editor: Ivan Tolj

Received: 18 February 2023

Revised: 2 April 2023

Accepted: 19 April 2023

Published: 5 May 2023



Copyright: © 2023 by the authors. Licensee MDPI, Basel, Switzerland. This article is an open access article distributed under the terms and conditions of the Creative Commons Attribution (CC BY) license (<https://creativecommons.org/licenses/by/4.0/>).

1. Introduction

As the world becomes increasingly aware of the environmental impact of internal combustion engine (ICE) cars, alternative technologies have emerged to replace them. One promising technology is the fuel cell electric vehicle (FCEV), which uses hydrogen and oxygen to produce electricity, emitting only water vapor as a byproduct. FCEVs have been in development for decades, but only recently have it begun to gain traction as a viable alternative to ICE cars [1]. FCEVs offer several advantages over traditional gasoline or diesel vehicles. First and foremost, they emit zero greenhouse gases and pollutants, making them a cleaner transportation option [2]. Additionally, FCEVs have a longer range than battery electric vehicles (BEVs) and can be refueled quickly, making them more practical for long-distance driving. They also have the potential to reduce dependence on oil and increase energy security. In addition, the principal function of a FC-HEV is to convert the energy from hydrogen fuel and oxygen in the air into electrical energy through an electrochemical reaction in a fuel cell [3]. This electrical energy is then used to power the vehicle's electric motor, which drives the wheels. In a FC-HEV, the fuel cell serves as the primary power

source; however, the performance of fuel cells can be limited by slow dynamics in the air compressor and manifold filling, especially during high-demand situations such as rapid acceleration or high-speed driving [4]. To address this, batteries and supercapacitors have emerged as key technologies in electric vehicle powertrains, as they offer high energy and power density, respectively. By combining these technologies, electric vehicles can potentially achieve the benefits of both, providing sustainable and efficient transportation. For this reason, researchers and manufacturers are paying significant attention to FC-HEVs (fuel-cell hybrid electric vehicles) [5]. Hence, when designing a hybrid storage system for a fuel cell electric vehicle, one of the key challenges is determining the appropriate sizing and type of components to use. This is because the hybrid storage system needs to balance the tradeoff between energy density, power density, cost, and weight. In addition, the choice of battery and supercapacitor components plays a crucial role in determining the efficiency of electric vehicles. Lithium-ion batteries, for example, are widely used due to their high energy density, longer lifespan, and relatively low self-discharge rate. On the other hand, supercapacitors, such as maxwell, have high power density and quick charge and discharge capabilities, which makes them ideal for regenerative braking and providing power during acceleration. The efficiency of electric vehicles is dependent on various factors, including the energy storage system, the motor, and the overall design of the vehicle [6]. Therefore, the proper selection of battery and supercapacitor components can significantly impact the efficiency of the electric car. To address these challenges, researchers have proposed various approaches, including analytical and simulation-based methods, to size and optimize the hybrid storage system such as [7–9]. However, all of these studies were examining the optimal sizing and energy management to choose the type of component in a discrete way. In this paper, a new energy management strategy was developed for FCHEVs that controls each mode individually. This strategy determines the optimal size using the MOPSO algorithm to optimize the FC, SC and battery size to meet driving conditions while reducing overall fuel consumption. Four driving cycles from the FCHEV application database were used to analyze the effects of driving conditions on fuel consumption. Optimal batteries and supercapacitors were chosen to drive the SFTP-SC03 to achieve a lower multi-objective function value.

The sections of the article are as follows. The modeling and validation of the FCHEV are presented in Section 1. In Section 2, the energy management strategy is proposed for the optimal sizing of the FCHEV. In Section 3, we present a simplified explanation of the MOPSO algorithm. Then, in Section 4, simulations are presented via the vehicle application to discuss the results obtained in Section 5. Finally, the conclusion and recommendations for future work are summarized in Section 6.

2. Modeling of the FCHEV

2.1. Vehicle Dynamic Model

In Figure 1, the fuel cell, battery, and super-capacitor are all connected by a DC/DC converter and combined by a DC/DC link, and then connected to the motor by a DC/AC converter [10].

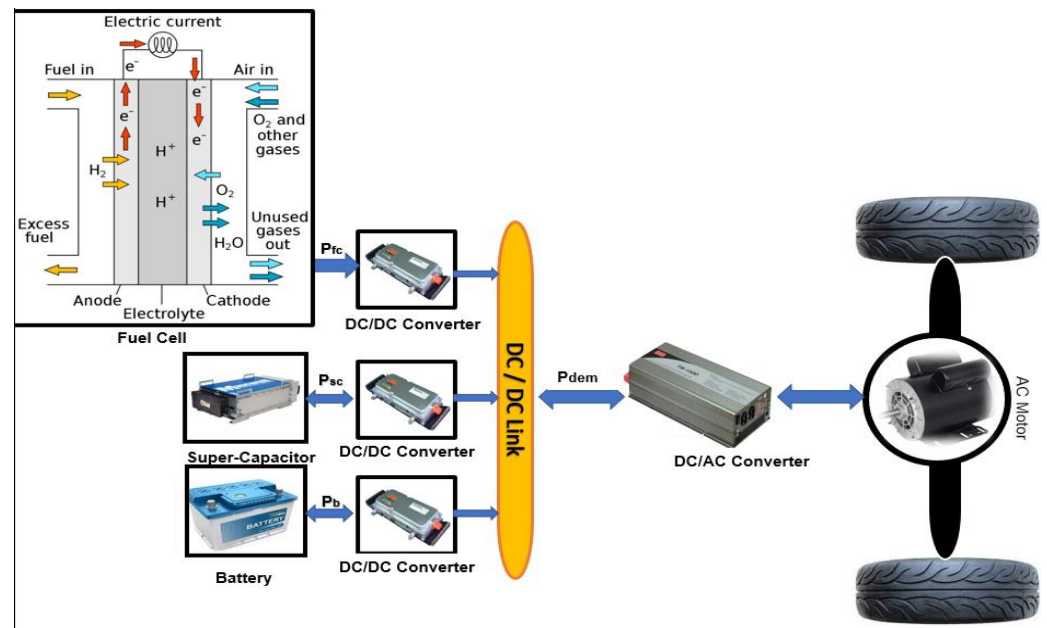


Figure 1. Topology of FCHEV.

The power required can be calculated as the sum of the acceleration power P_{acc} , power due to rolling resistance (P_{roll}), power due to air resistance (P_{aero}), and power due to climbing a slope (P_{gx}) by using Equations (1)–(5) [11].

$$P_{motor}(t) = P_{aero}(t) + P_{roll}(t) + P_{gx}(t) + P_{acc}(t), \quad (1)$$

$$P_{aero}(t) = 0.5 \rho A C_x V_{veh}(t)^3, \quad (2)$$

$$P_{acc}(t) = M \alpha(t) V_{veh}(t), \quad (3)$$

$$P_{roll}(t) = M g (C_0 + C_1 V_{veh}(t)^2) V_{veh}(t), \quad (4)$$

$$P_{gx}(t) = M g \sin(\beta(t)) V_{veh}(t), \quad (5)$$

where in M is the vehicle weight, the vehicle’s velocity is denoted by V_{veh} , ρ denotes the density of air, C_x is the vehicle aerodynamic drag coefficient, A represents the vehicle’s frontal area, α denotes the vehicle’s acceleration, the static rolling resistance coefficient is denoted as C_0 , the dynamic rolling resistance coefficient is denoted as C_1 , the gravitational acceleration is denoted by g , and β denotes the road slope.

The power required for an electric motor with a fuel cell, a battery, and a supercapacitor may be estimated using the vehicle’s longitudinal dynamic equation, which is shown in Equations (6) and (7) [12].

$$\begin{cases} P_{dem}(t) = \frac{P_{motor}(t)}{\eta_{motor}}, \text{ if } \frac{d}{dt} V_{veh}(t) > 0 \\ P_{rec}(t) = P_{motor}(t) \cdot \eta_{motor}, \text{ if } \frac{d}{dt} V_{veh}(t) < 0 \end{cases}, \quad (6)$$

$$P_{produit}(t) = P_{fc}(t) + P_b(t) + P_{sc}(t), \quad (7)$$

where P_{dem} represents the vehicle demand power when the acceleration mode meaning $\frac{d}{dt} V_{veh}(t) > 0$, $P_{rec}(t)$ represent recovered power from the motor when the braking mode meaning $\frac{d}{dt} V_{veh}(t) < 0$, $P_{produit}$ represent produced power by fuel cell, battery, and supercapacitor, η_{motor} represents the electric motor efficiency, and P_{fc} , P_b , and P_{sc} represent

the power of the fuel cell, battery, and supercapacitor, respectively [10]. The parameters that were used in the application of the FCHEV are shown in Table 1.

Table 1. FCHEV characteristics.

Parameter	Value
Vehicle mass (kg)	950
Vehicle frontal area (m ²)	1.75
Air density (ρ) (kg/m ³)	1.5
Vehicle aerodynamic drag coefficient (C_x) (m ²)	0.3
Static rolling resistance coefficient (C_0)	0.008
Dynamic rolling resistance coefficient (C_1)	1.6×10^{-6}
Electric motor efficiency (η_{motor}) (%)	0.95

2.2. Fuel-Cell Modelling and Experimental Validation

2.2.1. PEMFC Mathematical Model

A typical PEMFC is depicted in Figure 2. The electrochemical generator consists of three major components: a solid membrane (typically made of NafionTM material) and two metallic plates known as the anode and the cathode. These are the locations where hydrogen and oxygen react, respectively [13]. When an outside load is connected, hydrogen atoms divide into electrons and protons, resulting in an electrical current. As a result of these electrochemical processes, the cathode releases heat and water vapor.

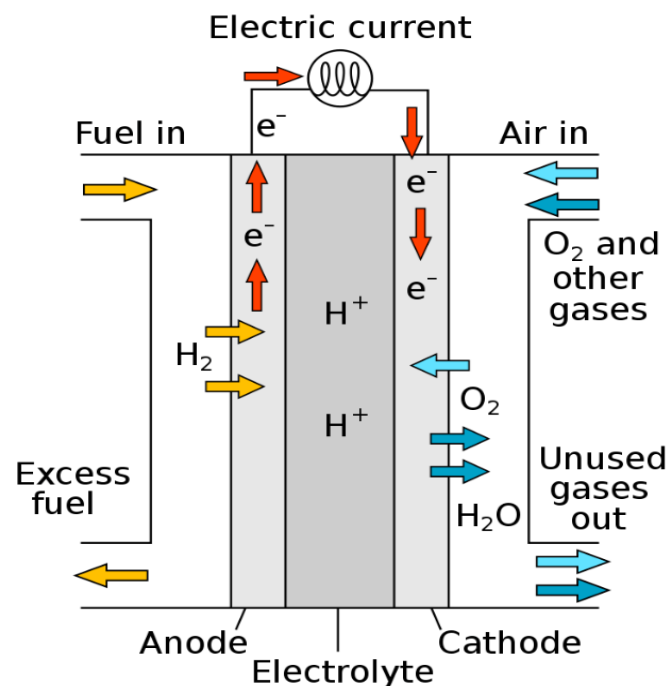


Figure 2. Inner view of PEMFC.

The output voltage of the FC, V_{FC} , is the variation between its reversible open-circuit voltage and its reductions in internal voltage, including the loss or reduction in ohms, activation, and concentration. The nonlinear functions of the FC chemical reactions, temperature, and current are these losses. The essential term for the PEMFC voltage was illustrated in a previous study [14]. We can calculate the output power of the FC related to the output voltage V_{FC} , I (A), the FC current, and the number of FC NB_{fc} using Equations (8)–(10):

$$P_{FC} = NB_{fc} \times (V_{FC} \times I), \quad (8)$$

$$V_{FC} = E_{Nernst} - V_{act} - V_{ohm} - V_{conc}, \quad (9)$$

$$V_{FC} = N_s \times \left[\left\{ 1.229 - 0.85 \times 10^{-3} \times (T - 298.15) + 4.3085 \times 10^{-5} \times T \times \ln(P_{H2,an} \times \sqrt{P_{O2,ca}}) \right\} + \left\{ [\xi_1 + \xi_2 \times T + \xi_3 \times T \times \ln(C_{O2}) + \xi_4 \times T \times \ln(I)] \right\} + \left\{ \beta \times \ln\left(1 - \frac{J}{J_{max}}\right) \right\} - \left\{ (R_m + R_c) \times I \right\} \right], \quad (10)$$

where V_{FC} is the output voltage of the PEMFC generator, and N_s is the number of cells assembled in series. E_{Nernst} is the no-load voltage in an open-circuit thermodynamic balance. V_{act} is the activation voltage resulting from the sluggish kinetic reactions occurring on the surface of the anode and cathode, V_{con} is the concentration voltage drop, and V_{ohm} is the ohmic voltage drop caused by the resistance values of the membrane and metal contacts, $R_m(\Omega)$ and $R_c(\Omega)$, respectively. T is the cell temperature (K), and ξ_1 , ξ_2 , ξ_3 , and ξ_4 are semi-coefficients based on electrochemistry. $P_{H2,an}$ and $P_{O2,ca}$ are the partial pressure values of the hydrogen and oxygen (atm) entering the anode and cathode, respectively. I and J are the current (A) and current density (A/cm²) of the PEMFC stack, respectively. C_{O2} is the concentration of oxygen on the surface of catalysis (mol/cm³). β is an empirical parametric coefficient in volts. J_{max} is the maximum allowable current density. The concentration C_{O2} and resistance R_m are calculated using Equations (11) and (12), respectively [15,16]:

$$C_{O2} = \frac{P_{O2,ca}}{5.08 \times 10^6} \times \exp\left(\frac{498}{T}\right), \quad (11)$$

$$R_m = \frac{l \times \rho_M}{A} = \frac{181.6 \left[1 + 0.03 \left(\frac{I}{A}\right) + 0.062 \left(\frac{T}{303}\right)^2 \left(\frac{I}{A}\right)^{2.5} \right] \times l}{A \times \left[\lambda - 0.634 - 3 \times \left(\frac{I}{A}\right) \right] \times \exp\left[4.18 \left(\frac{T-303}{T}\right) \right] \times A}, \quad (12)$$

where ρ_M stands for the resistivity of the membrane (Ω cm), and l is the thickness of the membrane (cm). A is the activation surface of the stack (cm²), and λ is an adjustable fitting parameter influenced by the material properties of the membrane [15,17]. The fuel consumption of the fuel cell can be calculated according the following Equation (13):

$$\dot{m} = \frac{1}{E_{low,H2}} \int_{t_1}^{t_2} \frac{P_{fc}(t)}{\eta_{fc}} dt, \quad (13)$$

where \dot{m} is the fuel consumption per second, $E_{low,H2} = 120$ MJ/kg is the lower heating value of hydrogen [18,19], P_{fc} is the output power of the fuel cell (FC) system, and η_{fc} is the efficiency of the FC system presented in Figure 3, where net power = $P_{fc}/P_{nominal}$.

2.2.2. Validation of NedStack PS6 PEMFC Stack Modeling in FCHEV Application

In this section, the mathematical model is validated by NedStack PS6 PEMFCs by Fawzi et al. [20,21].

In this study, we used the PS6 PEMFC stack model at 26 kg, where the fuel cell system cost was USD 53/kW and the hydrogen price (μ_{fc}) was USD 2/kg [22]. The results of Fawzi et al. [20] were used to acquire data for this PS6 PEMFC-6kW. The aforementioned PEMFC had a rated power of 6 kW and comprised 65 cells stacked in series. The highest current density J_{max} was 1.2 A/cm², whereas the membrane thickness and cell active area (A) were 178 μ m and 240 cm², respectively. Furthermore, the maximum thermal current of this system was 225 A. The $P_{H2,an}/P_{O2,ca}$ values were maintained constant at 1/1 atm, and the temperature of this stack was 343.15 K. Figure 4 depicts the predicted and experimentally obtained (I/V) and (P/V) curves corresponding to the PS6 PEMFC in the FCHEV application. We used the optimum parameter obtained by Fawzi et al. and shown in Table 2 for the PEMFC mathematical model validation process of the simulated vehicle

(mass: 950 kg and frontal area: 2.75 cm²) based on a HESS (Maxwell BCAP0003 SC and Li-ion battery).

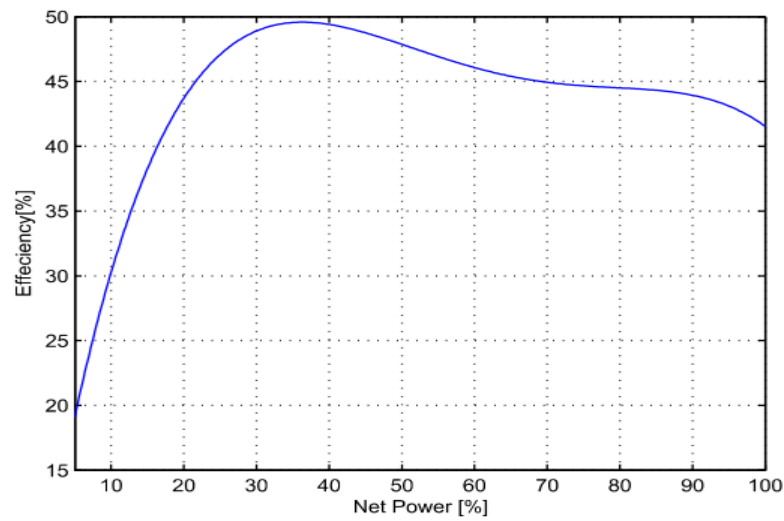


Figure 3. Fuel cell system efficiency.

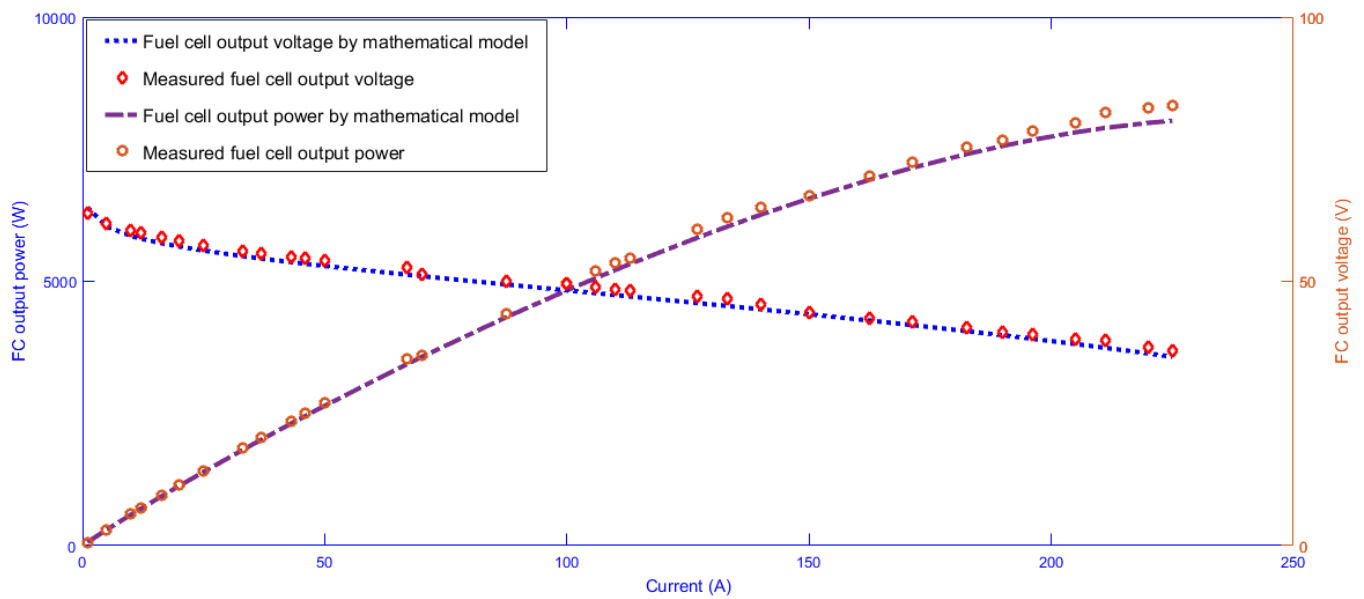


Figure 4. I/V, I/P plot for NedStack PEMFC.

Table 2. The optimal parameters for PEMFC.

Parameter	NedStack PS6, Fawzi et al. [20].
ζ_1	-0.8535
$\zeta_2 \times 10^{-3}$	2.4316
$\zeta_3 \times 10^{-5}$	3.7545
$\zeta_4 \times 10^{-5}$	-9.5400
λ	13.0802
β	0.0136
$R_c \times 10^{-4}(\Omega)$	1

The optimum parameter values for the PEMFC model used in the FCHEV application database are shown in Table 2.

2.3. Hybrid Energy Storage System (HESS) Modeling

2.3.1. Supercapacitor Modeling

A supercapacitor can be used when it is desired to increase the velocity of the vehicle rapidly. The energy supply by the supercapacitor can be approximated by Figures 5 and 6 [23]:

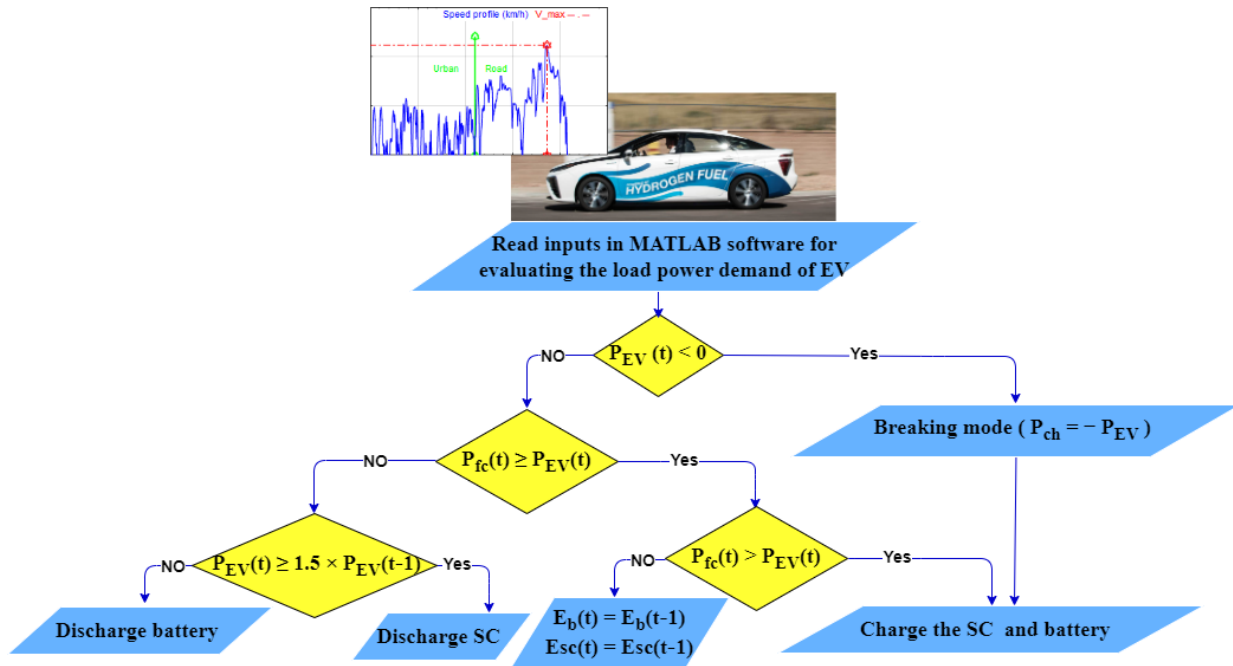


Figure 5. The main flowchart for FCHEV.

The minimum state of discharge (E_{sc}^{min}) related to the dump of discharge (DOD_{sc}) and the maximum state of discharge (E_{sc}^{max}) are represented in Equation (14):

$$E_{sc}^{min} = (1 - DOD_{sc}) \times E_{sc}^{max}, \tag{14}$$

where E_{sc} is the energy of the SC bank. In every second (t), the supercapacitor’s state of charge is controlled via the min and max values of supercapacitor capacity, E_{sc}^{min} and E_{sc}^{max} , which can be expressed as in Equations (15)–(17).

$$E_{sc}^{min} \leq E_{sc}(t) \leq E_{sc}^{max}, \tag{15}$$

$$SOC_{sc}(t) = \frac{E_{sc}(t)}{E_{sc}^{max}}, \tag{16}$$

$$E_{sc}^{max} = V_{sc}^{max} \cdot I_{sc}. \tag{17}$$

2.3.2. Battery Bank Modeling

A battery bank is utilized when the electricity generated by a fuel cell is insufficient, and the energy supply provided by the battery bank can be approximated using flowchart of the charging/discharging mode in Figure 7 [23].

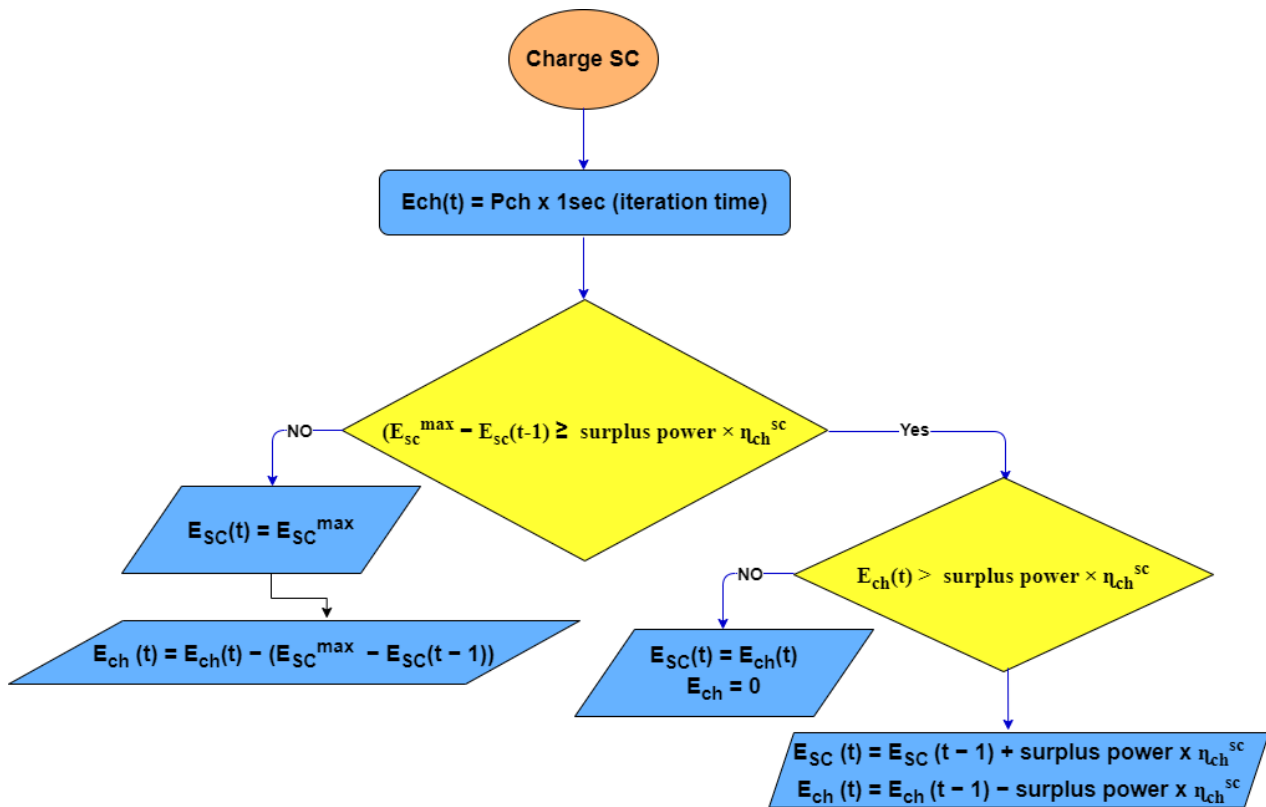


Figure 6. The main flowchart for charging SC.

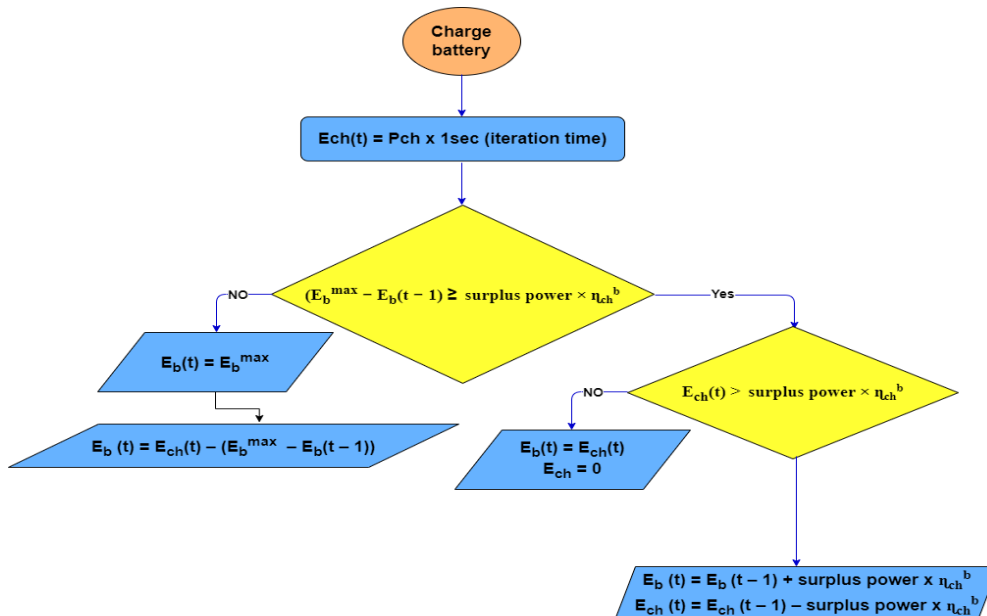


Figure 7. The main flowchart for charging battery.

The minimum state of discharge (E_b^{min}) related to the dump of discharge (DOD_b) and the maximum state of discharge (E_b^{max}) of the battery can be determined using Equation (18):

$$E_b^{max} = (1 - DOD_b) \times E_b^{max}, \tag{18}$$

where E_b is the energy of the battery bank. In every second (t), the battery's state of charge is controlled via the min and max values of battery capacity, E_b^{min} and E_b^{max} , which can be expressed as in Equations (19)–(21).

$$E_b^{min} \leq E_b(t) \leq E_b^{max}, \quad (19)$$

$$SOC_b(t) = \frac{E_b(t)}{E_b^{max}}, \quad (20)$$

$$E_b^{max} = V_b^{max} \cdot I_b. \quad (21)$$

The characteristics of the HESS used in the database for the FCHEV application are shown in Table 3 [24,25].

Table 3. HESS characteristics.

Parameter	Value for Battery Types					Value for SC Type		Unit
	Lithium	Li-ion	Na-NiCl ₂	Ni-MH	Li-S	Maxwell BCAP0003	ESHSR-3000CO	
Weight	10.35	11.5	12	20	13	13.8	11.8	Kg
Typical Cost(C_b, C_{sc})	150	165	170	190	200	5000	3500	USD/kWh
Maximum Voltage	78	75	71	75	72	800	650	V
Nominal Capacity	9.3	9.46	7.32	6.73	6.089	/	/	Ah
(Charge/Discharge) Current	/	/	/	/	/	100	100	A
Maximum SOC	100	100	100	100	100	100	100	%
Minimum SOC	20	20	20	20	20	20	20	%
Initial Charge	80	80	80	80	80	80	80	%
Charging/Discharging time	>1800	>1800	>1800	>1800	>1800	1–30	1–30	s
Charge/Discharge efficiency	0.9 /0.85	0.9 /0.85	0.9/0.85	0.9/0.85	0.9/0.85	0.9/0.85	0.9/0.85	/

3. Energy Management Strategy for Optimal Sizing of FCHEV

The management plan for the FCHEV is one of the most important aspects in designing an FCHEV. The primary energy management strategy flowchart is provided in Figure 5, and the indicated procedures * (a–d) are described in the flowcharts of charging the SC, charging the battery, discharging the SC, and discharging the battery in Figures 5–9. By using Equations (1)–(5), we can compute the power required by the car based on the speed load and vehicle parameters, and then investigate the signal of this energy to determine the power mode (braking mode or acceleration mode). In braking mode, the recovered engine energy is used to charge both the battery and the supercapacitor. In the scenario of acceleration mode, when the necessary energy is positive, there are two possibilities: either the fuel cell's energy is sufficient to meet the demand, or it is not. In case of the former, we charge both the supercapacitor and the battery after testing the charge for each of them, as shown in Figures 6 and 7. In the event that the energy of the fuel cell is insufficient to meet the energy demand, there are two options: in the case of a rapidly increasing energy demand (with an increased rate of 150%), we use the discharge of the supercapacitor after testing it, as shown in Figure 8, but in the case of a normal increase, we use the battery after it has been tested, as shown in Figure 9.

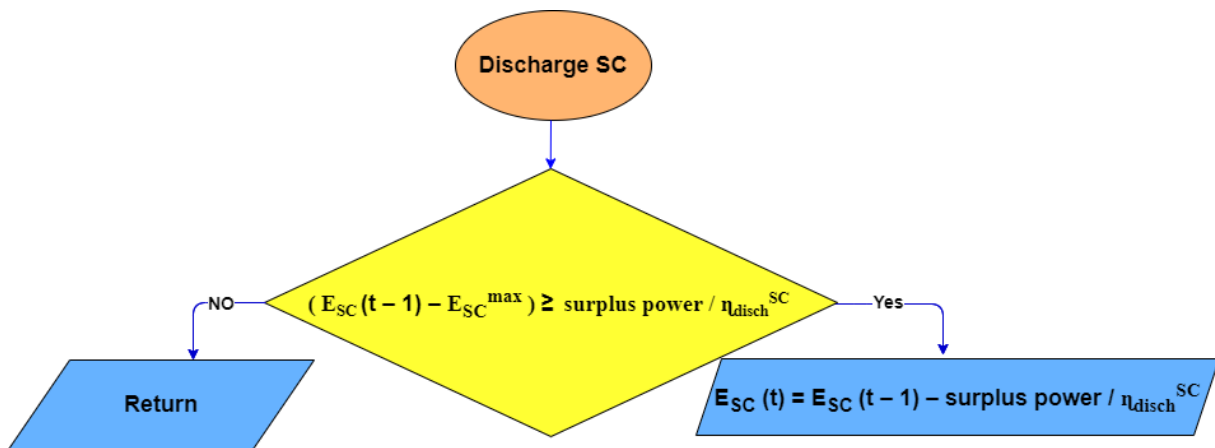


Figure 8. The main flowchart for discharging SC.

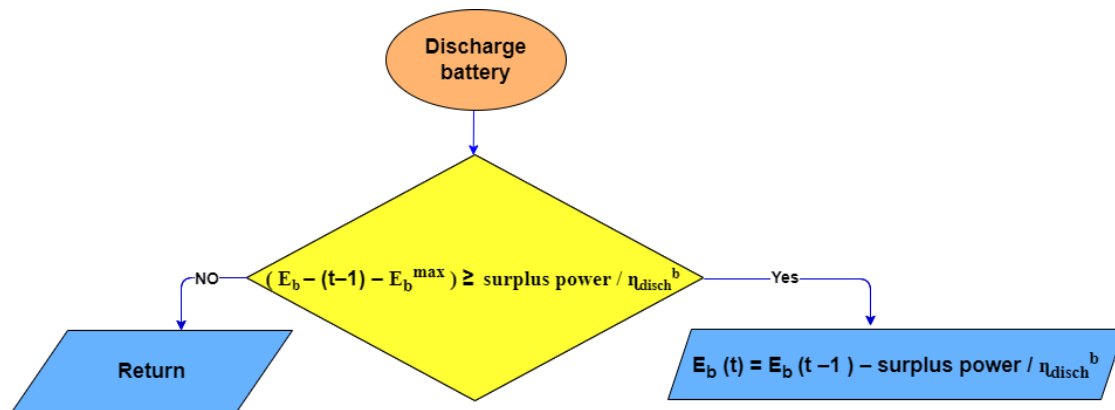


Figure 9. The main flowchart for discharging battery.

In the Figures, η_{ch}^{sc} and η_{disch}^{sc} are, respectively, the charging and discharging efficiency values of the SC bank in this paper, and the random η_{ch}^{sc} and η_{disch}^{sc} values were selected, respectively, as 90% and 85%. η_{ch}^b and η_{disch}^b are the charging and discharging efficiency values of the battery bank in this paper, and η_{ch}^b and η_{disch}^b were considered to be 90% and 85%, respectively.

4. Multi Objective Particle Swarm Optimization (MOPSO) for Optimal Sizing of FCHEV

PSO techniques have attracted considerable interest in the field of power systems and have been successfully applied to a variety of difficult optimization problems in power systems. PSO-based algorithms' primary advantages include straightforward concept, ease of implementation, robust parameter control, and greater computational efficiency compared to other mathematical algorithms and empirical optimization techniques. This article discusses the use the PSO approach to determine the optimal component sizes (FC, Battery, and SC), thereby increasing the vehicle's efficiency and lowering its cost. The concept of swarm intelligence is founded on the interaction of swarm groups and evolutionary computation. The best two values in the PSO algorithm define the position of each particle. The first is the particle's best value after it has been saved. This is referred to as the "local best." Additionally, each particle has a position that indicates the value of variables as well as a velocity that propels it toward local and global bests. A fitness function is a special case of an objective function in that it seeks the optimal solution among all possible solutions. Additionally, the multi-objective function considers the investment cost, operating cost, and component weight. A PSO algorithm is composed of three essential steps [26]:

- ❖ Estimate the fitness of every particle.
- ❖ Update the local and global best fitness and position.
- ❖ Update the velocity and position of all particles.

While the PSO algorithm is running, each object retains its best fitness value. The particles with the best fit value compared to other particles are also calculated and updated during each iteration. The process is repeated until the algorithm meets one of the stopping criteria, such as the number of iterations or predefined target fitness values. The position of each particle in the swarm is updated according to Equation (22):

$$X_{k+1}^i = X_k^i + v_{k+1}^i \quad (22)$$

In iteration k , X represents particle positions, and v represents particle velocities. The velocity can be calculated using Equations (23)–(25):

$$v_{k+1}^i = k \times \left[v_k^i + C_1 r_1 (P_k^i - X_k^i) + C_2 r_2 (P_k^g - X_k^i) \right], \quad (23)$$

$$K = \frac{2}{2 - \phi - \sqrt{\phi^2 - 4\phi}}, \quad (24)$$

$$\phi = C_1 - C_2, \quad \phi > 1, \quad (25)$$

where P^i represents the best local position of the particle, P^g represents the its best global position, C_1 and C_2 represent the cognitive and social factors, respectively, and r_1 and r_2 are random values between 0 and 1. The difference between C_1 and C_2 is usually close to 2, and it affects the size of the particle's stride towards the local and global bests, respectively. In this study, both values were considered to be 2 to attract the particle equally to the optimal positions.

V_k^i , known as inertia, acts as the particle moves in the same direction at the same speed. $C_1 r_1 (P_k^i - X_k^i)$, is referred to as the cognitive element and causes the particle to return to a position where it has experienced greater local fitness. $C_2 r_2 (P_k^g - X_k^i)$ represents the social components which cause the particle to return to the most appropriate area the swarm has discovered thus far and follow the top neighbor's direction before each iteration. If $C_2 > C_1$, the particle is more attracted to local best positions; if $C_2 < C_1$, the particle is more attracted to the global best position.

4.1. Objective Function Formulation:

In this study, the multi-objective optimization process aimed to reduce the total operating cost and optimize the sizing of the components in the FCHEV simultaneously, mainly for the fuel cell, battery, and supercapacitor. Therefore, we aimed to increase the performance of the FCHEV. The multi-objective function can be defined as in Equation (26) [22].

$$\begin{aligned} \text{Min OF} = & \left[N_{batt} * C_b + N_{sc} * C_{sc} + N_{fc} * \psi * C_{fc} \right] \\ & + \left[N_{batt} * w_b + N_{sc} * w_{sc} + N_{fc} * \psi * w_{fc} \right] \\ & + \left(\mu_{fc} \left[\int_{t_1}^{t_2} P_{fc} dt * \varepsilon \right] + \mu_b \left[\int_{t_1}^{t_2} P_b dt \right] \right), \end{aligned} \quad (26)$$

where C_b , C_{sc} , and C_{fc} are the cost values of the battery, supercapacitor, and FC, respectively; w_b , w_{sc} , and w_{fc} are the weights of the battery, supercapacitor, and FC, respectively, and the price of hydrogen is μ_{fc} in USD/kg according to the DOE 2020 [5]. $\int_{t_1}^{t_2} P_{fc} dt$ represents the energy required by the FC each second. We used the factor ε , where $\varepsilon = \frac{3.6}{0.45 * 119.96}$, μ_b is the price of electricity in USD/kWh, and P_b is the power demand of the battery. The factor ψ is used to make the FC operate at 25–40% of its rated power (maximum efficiency region). Therefore, the multi-objective function includes the investment cost, the operating cost, and the weights of the components.

4.2. Optimization Parameter Settings

The multi-objective optimization problem was created in order to reduce the investment cost, the component weights, and the operating cost. Table 4 shows the optimization parameter setting values after taking into account the maximum number of iterations, minor constraints, and major constraints [22].

Table 4. Optimization parameter settings.

Parameter	Value
Population size (N)	30
Maximum number of iterations (W)	100
$[NB_{fc}^{\min}, NB_{fc}^{\max}]$	[0, 10]
$[NB_{sc}^{\min}, NB_{sc}^{\max}]$	[0, 10]
$[NB_b^{\min}, NB_b^{\max}]$	[0, 10]
Hydrogen price μ_{fc}	USD 2/kg
Electricity price μ_b	USD 0.138/kWh

5. Simulation and Results

In this section, we examine the possible use of FCHEV in two different case situations. First, we examine the ways in which different driving cycles (SFTP-SC03, NEDC, Artemis, and WLTP) affect vehicle economy, taking into account aspects such as hydrogen use, operating costs, and component mass. Second, we choose the best hybrid storage solution based on battery and supercapacitor properties such as capacity, weight, and cost.

5.1. FCHEV Simulation in Different Driving Cycle

Figure 10A–D depicts the effect of speed profile on fuel consumption in the Artemis, WLTP, NEDC, and SFTP-SC03 driving cycles. In comparison to different driving cycles, the SFTP-SC03 driving cycle has a low fuel consumption of about 5.61 g/km shown in Figure 10D. This is because the SFTP-SC03 driving cycle includes low acceleration processes, causing the system to downsize the fuel cell by about 35.37 kW due to the low power demand on the engine side, as shown in Figure 11D. Note that although the maximum speed value in the Artemis driving cycle of 111.5 km/h as shown in Figure 10A is lower than that of the NEDC driving cycle of 120 km/h as shown in Figure 10C, the choice of fuel cell size in the Artemis driving cycle, it was larger than the NEDC driving cycle, and this is due to the magnitude of the accelerations in the Artemis driving cycle, which was very large, which affected the energy required by the fuel cell as shown in Figure 11A compared to the NEDC drive cycle shown in Figure 11C, this interpretation is confirmed by the comparison of the NEDC driving cycle in Figures 10C and 11C with the SFTP-SC03 driving cycle in Figures 10D and 11D, so we note the system taking a larger fuel cell size in the SFTP-SC03 driving cycle, although it has the highest speed in The NEDC drive cycle is very large compared to the SFTP-SC03 drive cycle. Comparing the results also for the WLTP driving cycle shown in Figure 10B with other driving cycles shows that this cycle took the highest value for fuel consumption as well as the maximum energy value for the fuel cell, and this is mainly due to the large acceleration ratio shown in Figure 10B, which increased the percentage The energy required from the EV is as shown in Figure 11B, which increases fuel consumption, and make the system give more size for the FC. The analysis of the results reveals that various factors influence a vehicle's fuel use. To begin, when the vehicle moves through the air, it encounters air resistance, known as aerodynamic drag. The faster the vehicle's speed, the greater the aerodynamic drag, resulting in increased fuel consumption. Second, rolling resistance created by road tires impacts fuel consumption. Higher speeds result in increased rolling resistance, which increases fuel consumption. Furthermore, engine efficiency has a significant impact on fuel consumption. Engines

perform best in the low to mid-range of RPM. As the vehicle’s speed increases, the engine may have to work harder, resulting in decreased efficiency and increased fuel consumption. Finally, transmission gearing influences fuel consumption. Lower gears perform better at slower speeds, whereas higher gears perform better at faster speeds. As a result, fuel usage might vary depending on the vehicle’s speed and gearing. The results are summarized in Table 5.

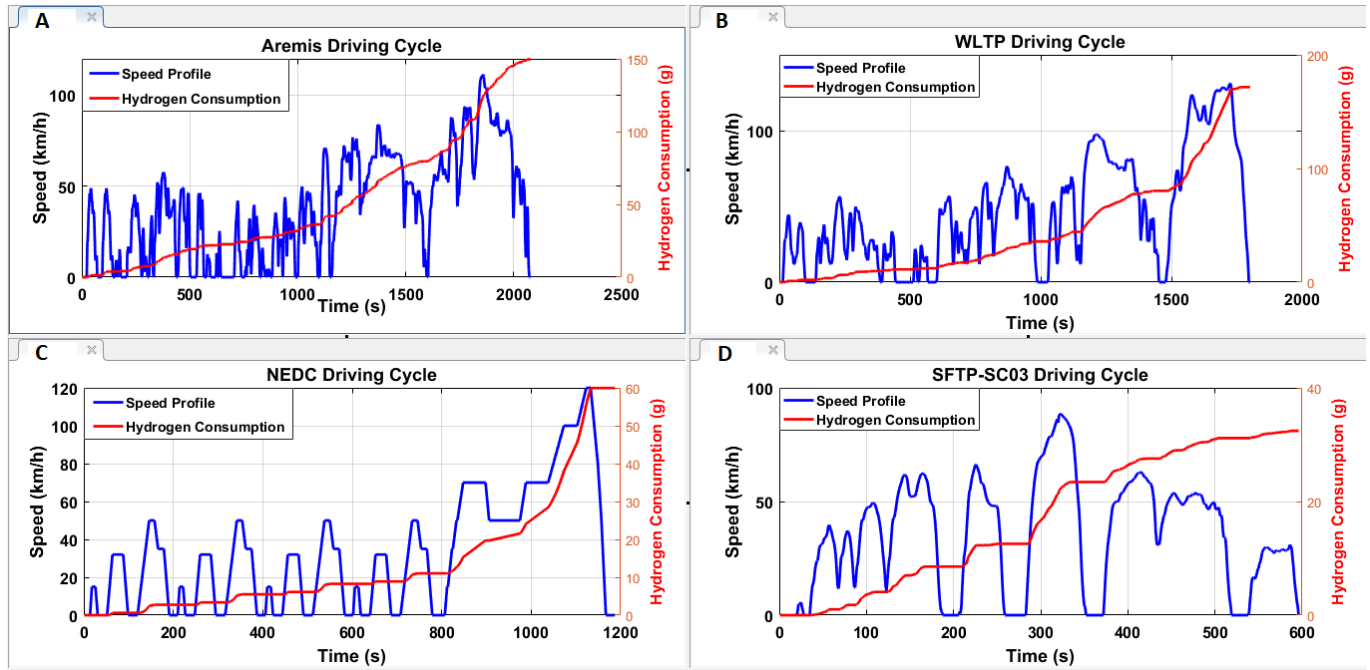


Figure 10. H₂ consumption with different driving cycles.

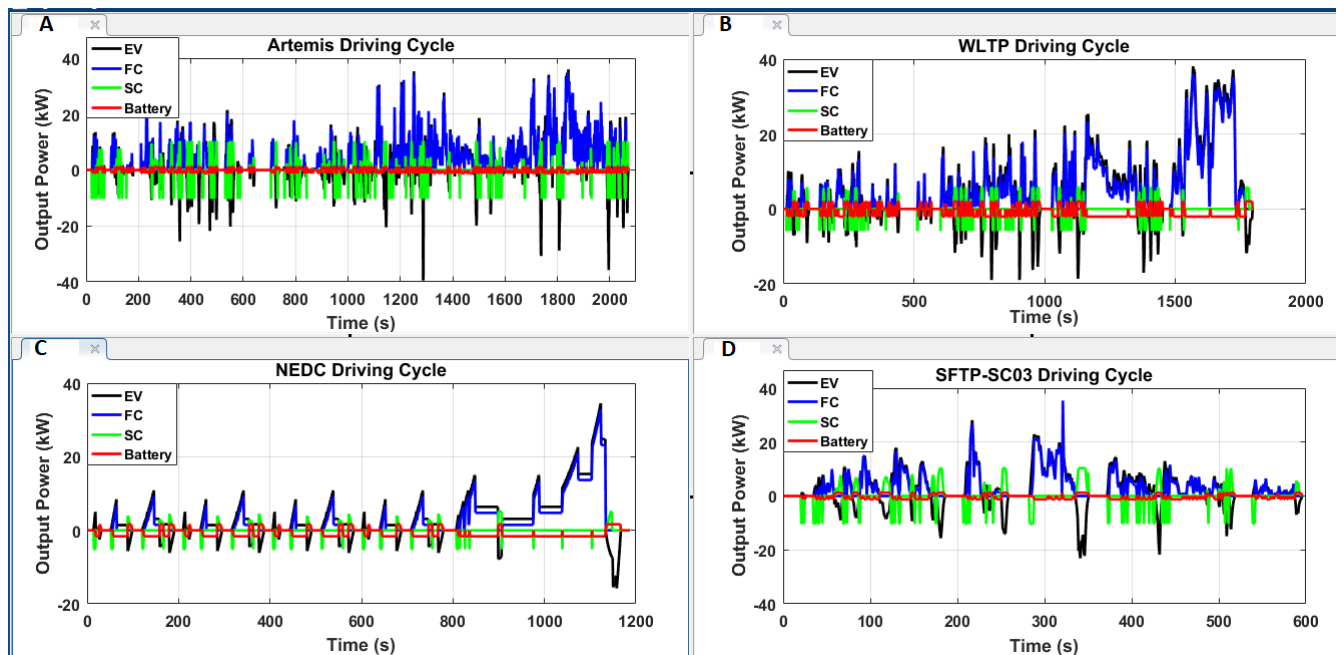


Figure 11. Output power results in different driving cycles.

Table 5. Multi-Objective PSO Results.

Decision Variables	Driving Cycles			
	Artemis	WLTP	NEDC	SFTP-SC03
Distance (km)	22.14	23.26	10.9314	5.78
Max Speed (km/h)	111.5	131.3	120	88.5
Average Speed (km/h)	38.37	46.49	33.1533	34.91
FC max Power (kW)	35.9446	38.1160	34.5545	35.3765
Number of batteries	3	5	3	3
Number of SCs	2	3	1	2
Fuel Consumption (g/km)	6.7589	7.3799	5.8761	5.61
Operating Cost (USD/km)	3.44×10^3	2.63×10^3	1.21×10^3	1.26×10^3
Components weight (kg)	165.62	220.37	151.82	165.62

5.2. Choosing the Best Battery with the Best SC for FCHEV

Figure 12A,B show the simulation results for the ESHR and Maxwell SC types when fuel consumption is considered. In addition, Figure 12C,D show the simulation results for the ESHR and Maxwell SC types when the running cost is considered respectively. Furthermore, the weight, cost, and capacity of each battery and supercapacitor are distinguishing features. The PSO algorithm evaluated the optimal fitness function value based on this information and the driving conditions, and the battery type with the lowest fitness function value was picked as the best alternative. Figure 12A,D presents the comparison results between the different batteries with ESHSR SC, it was clear that using a Lithium-Ion battery with a nominal capacity of 9.46 Ah, a maximum voltage of 75 V, and a cost of 165 USD/kWh resulted in the least amount of fuel consumption by about 29.27 g given in Figure 12A and the lowest operating cost 6838 are presented in Figure 12C for the electric vehicle in the SFTP-SC03 driving cycle. It is worth noting that the battery's huge capacity had the greatest impact on reducing hydrogen consumption, as it was critical in decreasing the fuel cell's operation and, as a result, lowering the rate of hydrogen consumption and operating expenses. After selecting the best type of battery, namely Li-ion, for the driving conditions in the first case study, we selected the best type of supercapacitor (ESHRSR-3000CO or Maxwell BCAP0003) for the driving conditions with the lowest fitness function value in the second case study. It should be mentioned that the Maxwell BCAP0003 with Lithium-Ion battery is the best case for FCHEVs in a variety of driving scenarios. Despite the fact that the cost of ESHSR-3000CO SC (5000 USD/kWh) is lower than that of Maxwell BCAP (USD 3500/kWh), the adoption of Maxwell BCAP SC allowed for the lowest fuel consumption presents in Figure 12B and the lowest operating cost present in Figure 12D By the values (29.84 g and USD 6798) respectively compared to ESHSR-3000CO (29.97 g and USD 6834). This occurred owing to the high capacity of the Maxwell supercapacitor, which made fuel cell operation easier by lowering hydrogen consumption and operating costs by around 0.43% and 0.53%, respectively. With driving cycles of more than 600 s, the savings in fuel consumption and operating costs would be significant.

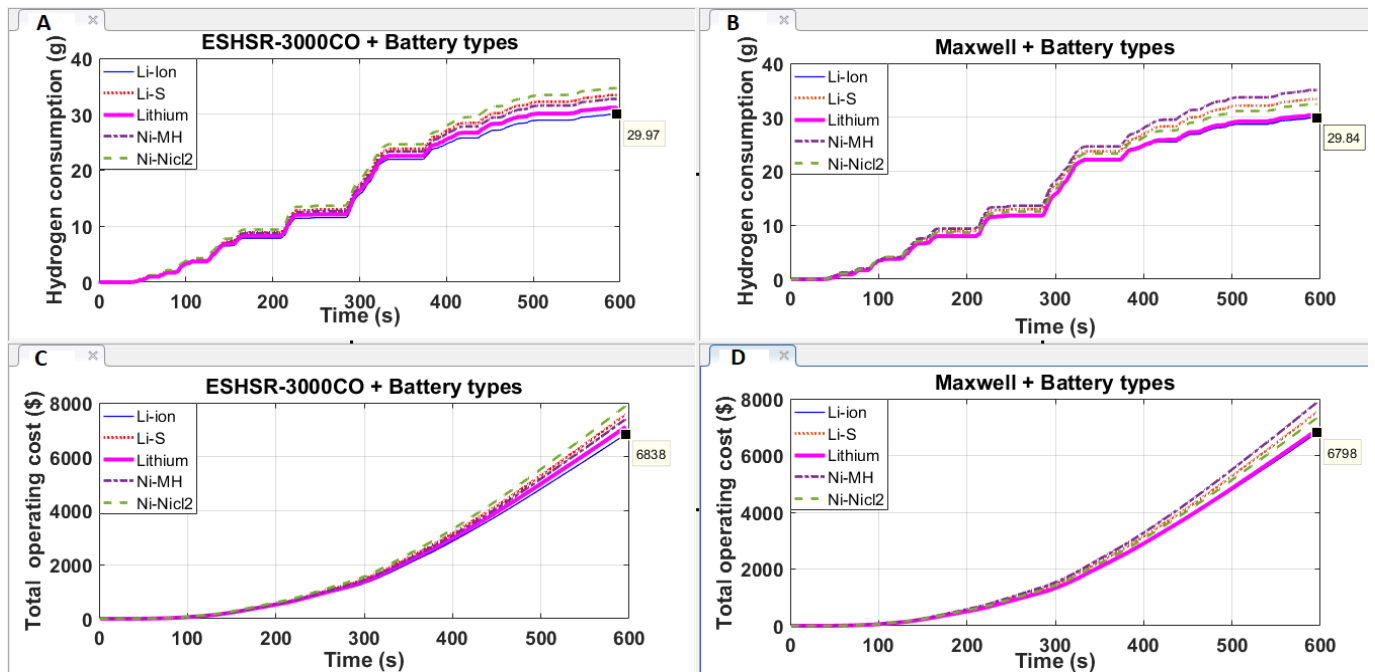


Figure 12. H₂ consumption and operating cost in different battery and SC in SFTP driving cycle.

5.3. Influence the Driving Cycle Condition on Vehicle Performance: A Comparative Study

A comparative study was added to the paper. The driving conditions and car characteristics, mainly vehicle weight 860 kg and vehicle frontal area 2.75, were applied, the same as for Bendjedia's study. Bendjedia et al. [19] showed the influence of the driving cycles on the ESS design in a comparison study using the New European (NEDC) driving cycle and the Assessment and Reliability of Transport Emission Models Inventory Systems (ARTEMIS) driving cycle, confirming that there is a big influence of the driving cycle on the ESS sizes and fuel consumption.

It is clear from reading results presented in Figures 13 and 14 that the fuel consumption in this study is lower than in Ahmed's study, as the results showed the contribution of using the new strategy in reducing the fuel consumption in the Artemis and NEDC and driving cycles by 20% and 49%, respectively. Although the maximum power of the fuel cell in this study is greater, this is due to the good control of the strategy during the simulation where the fuel cell consumes a percentage of the fuel according to the required effort. On the other hand, we note that the size of the fuel cell in this study is smaller. This is due to the optimal choice of the fuel cell model which was confirmed by two experimental studies for the two types of fuel cells where the ideal parameters were obtained for both studies, which made the results very strong.

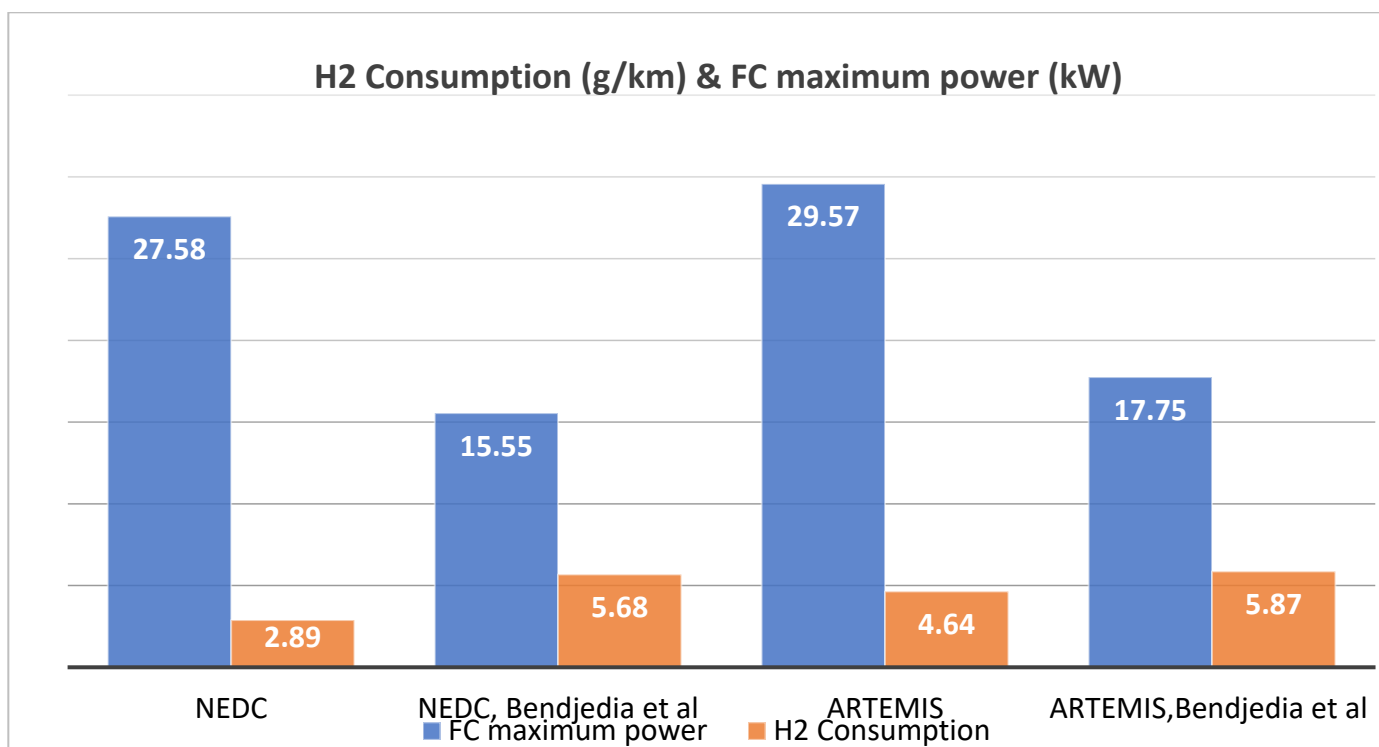


Figure 13. H2 consumption and FC maximum power results in different driving cycles [19].

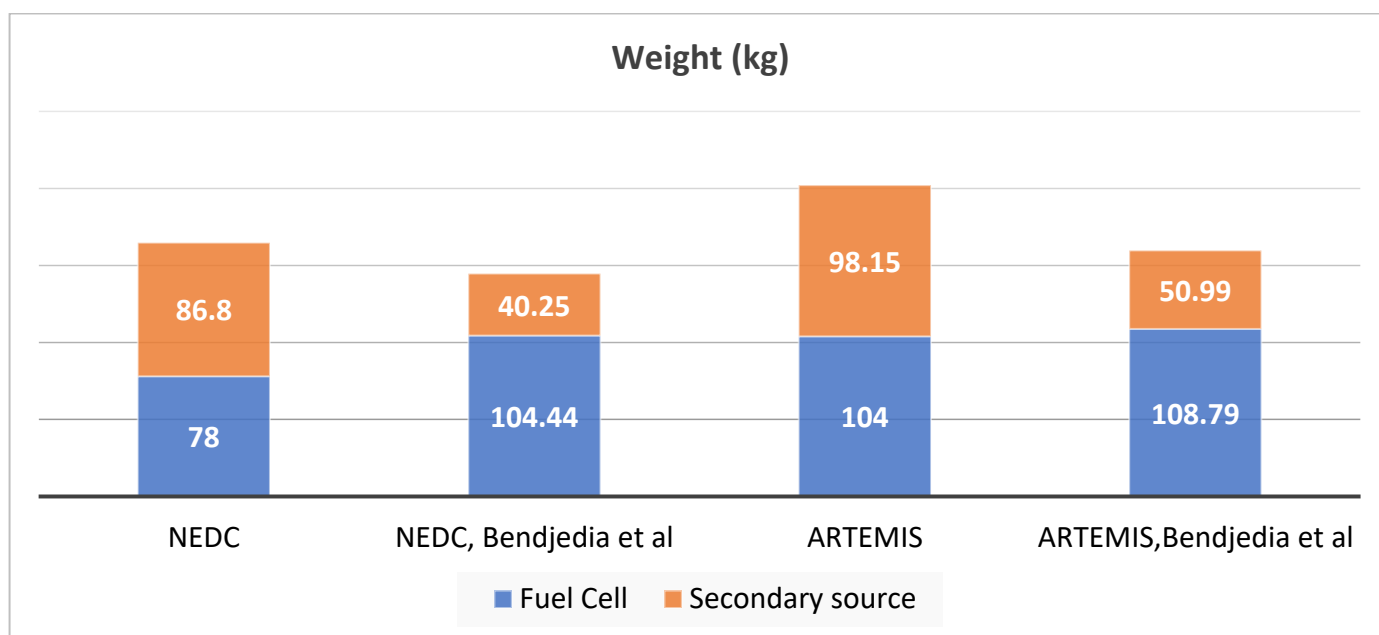


Figure 14. Component weight results in different driving cycles [19].

6. Conclusions and Recommendations for Future Studies

In conclusion, fuel cell hybrid electric vehicles (FCHEVs) represent an effective solution for reducing greenhouse gas emissions and conserving fossil fuels. This study employed the multi-objective particle swarm optimization algorithm in MATLAB code to optimize the sizing and energy management strategy at the same time for FCHEVs. The model was applied to four driving cycles, and the results showed that the selection of a Li-ion battery with Maxwell BCAP0003 as a secondary power source reduced fuel consumption by about 0.43% compared to ESHSR-3000CO. The study highlights the significant impact of

the type of secondary power sources, batteries, and driving conditions on the performance of FCHEVs. It is hoped that this research will pave the way for further studies to simulate fuel cell trains in cities such as Ouargla.

Author Contributions: Conceptualization, A.M.; Methodology, M.M.S.; Software, A.D.; Validation, B.N.; Formal analysis, A.D. and B.R.; Investigation, B.N.; Writing—original draft, A.D.; Project administration, A.D. All authors have read and agreed to the published version of the manuscript.

Funding: This research received no external funding.

Data Availability Statement: Data sharing is not applicable.

Conflicts of Interest: The authors declare no conflict of interest.

Nomenclature

Bi-DC	Bidimensional Direct Current
DOE	U.S. Department of Energy
FCHEV	Fuel Cell Hybrid Electric Vehicles
FCVs	Fuel Cell Vehicles
FCEVs	Fuel Cell Electric Vehicles
HESS	Hybrid Energy Storage System
ICEVs	Internal Combustion Engine Vehicles
MAS	Multi-Agent System
MOO	Multi-Objective Optimization
NBbatt	Number of batteries
NBFC	Number of Fuel-Cells
NBSC	Number of Supercapacitors
OC	Operating Cost
PEMFC	Proton-Exchange Membrane Fuel Cell
MOPSO	Multi-Objective Particle Swarm Optimization
SC	Supercapacitor
SOCb	State of charge of battery
SOCsc	State of charge of supercapacitor
DOD	Depth of Discharge

References

- Zheng, C.H.; Kim, N.W.; Cha, S.W. Optimal control in the power management of fuel cell hybrid vehicles. *Int. J. Hydrogen Energy* **2011**, *37*, 655–663. [\[CrossRef\]](#)
- Offer, G.J.; Howey, D.; Contestabile, M.; Clague, R.; Brandon, N.P. Comparative analysis of battery electric, hydrogen fuel cell and hybrid vehicles in a future sustainable road transport system. *Energy Policy* **2010**, *38*, 24–29. [\[CrossRef\]](#)
- Tanç, B.; Arat, H.T.; Baltacıoğlu, E.; Aydın, K. Overview of the next quarter century vision of hydrogen fuel cell electric vehicles. *Int. J. Hydrogen Energy* **2019**, *44*, 10120–10128. [\[CrossRef\]](#)
- Ahmadi, S.; Bathaee, S.M.T.; Hosseinpour, A.H. Improving fuel economy and performance of a fuel-cell hybrid electric vehicle (fuel-cell, battery, and ultra-capacitor) using optimized energy management strategy. *Energy Convers. Manag.* **2018**, *160*, 74–84. [\[CrossRef\]](#)
- Hung, Y.H.; Wu, C.H. An integrated optimization approach for a hybrid energy system in electric vehicles. *Appl. Energy* **2012**, *98*, 479–490. [\[CrossRef\]](#)
- Sulaiman, N.; Hannan, M.A.; Mohamed, A.; Ker, P.J.; Majlan, E.H.; Wan Daud, W.R. Optimization of energy management system for fuel-cell hybrid electric vehicles: Issues and recommendations. *Appl. Energy* **2018**, *228*, 2061–2079. [\[CrossRef\]](#)
- Song, Z.; Hofmann, H.; Li, J.; Han, X.; Zhang, X.; Ouyang, M. A comparison study of different semi-active hybrid energy storage system topologies for electric vehicles. *J. Power Sources* **2015**, *274*, 400–411. [\[CrossRef\]](#)
- Hu, X.; Johannesson, L.; Murgovski, N.; Egardt, B. Longevity-conscious dimensioning and power management of the hybrid energy storage system in a fuel cell hybrid electric bus. *Appl. Energy* **2015**, *137*, 913–924. [\[CrossRef\]](#)
- Zhu, T.; Wills, R.G.A.; Lot, R.; Ruan, H.; Jiang, Z. Adaptive energy management of a battery-supercapacitor energy storage system for electric vehicles based on flexible perception and neural network fitting. *Appl. Energy* **2021**, *292*, 116932. [\[CrossRef\]](#)
- Fu, Z.; Li, Z.; Si, P.; Tao, F. ScienceDirect A hierarchical energy management strategy for fuel cell/ battery/ supercapacitor hybrid electric vehicles. *Int. J. Hydrogen Energy* **2019**, *44*, 22146–22159. [\[CrossRef\]](#)

11. Feroldi, D.; Carignano, M. Sizing for fuel cell/ supercapacitor hybrid vehicles based on stochastic driving cycles. *Appl. Energy* **2016**, *183*, 645–658. [[CrossRef](#)]
12. Peng, J.; Wang, R.; Liao, H.; Zhou, Y.; Li, H.; Wu, Y.; Huang, Z. A real-time layer-adaptive wavelet transform energy distribution strategy in a hybrid energy storage system of EVS. *Energies* **2019**, *12*, 440. [[CrossRef](#)]
13. Page, K.A.; Rowe, B.W. An Overview of Polymer Electrolyte Membranes for Fuel Cell Applications. *Polym. Energy Storage Deliv. Polyelectrolytes Batter. Fuel Cells* **2012**, *1096*, 147–164. [[CrossRef](#)]
14. Chen, K.; Laghrouche, S.; Djerdir, A. Degradation model of proton exchange membrane fuel cell based on a novel hybrid method. *Appl. Energy* **2019**, *252*, 113439. [[CrossRef](#)]
15. Priya, K.; Rajasekar, N. Application of flower pollination algorithm for enhanced proton exchange membrane fuel cell modelling. *Int. J. Hydrogen Energy* **2019**, *44*, 18438–18449. [[CrossRef](#)]
16. Cheng, J.; Zhang, G. Parameter fitting of PEMFC models based on adaptive differential evolution. *Int. J. Electr. Power Energy Syst.* **2014**, *62*, 189–198. [[CrossRef](#)]
17. Benmouna, A.; Becherif, M.; Chen, J.; Chen, H.; Depernet, D. Interconnection and damping assignment passivity based control for fuel cell and battery vehicle: Simulation and experimentation. *Int. J. Hydrogen Energy* **2019**, *44*, 22467–22477. [[CrossRef](#)]
18. Li, C.Y.; Liu, G.P. Optimal fuzzy power control and management of fuel cell/battery hybrid vehicles. *J. Power Sources* **2009**, *192*, 525–533. [[CrossRef](#)]
19. Bendjedja, B.; Rizoug, N.; Boukhni, M. Influence of secondary source technologies and energy management strategies on Energy Storage System sizing for fuel cell electric vehicles. *Int. J. Hydrogen Energy* **2017**, *43*, 11614–11628. [[CrossRef](#)]
20. Fawzi, M.; El-Fergany, A.A.; Hasani, H.M. Effective methodology based on neural network optimizer for extracting model parameters of PEM fuel cells. *Int. J. Energy Res.* **2019**, *43*, 8136–8147. [[CrossRef](#)]
21. Zhou, X.; Qin, D.; Hu, J. Multi-objective optimization design and performance evaluation for plug-in hybrid electric vehicle powertrains. *Appl. Energy* **2017**, *208*, 1608–1625. [[CrossRef](#)]
22. Prasanthi, A.; Shareef, H.; Asna, M.; Asrul Ibrahim, A.; Errouissi, R. Optimization of hybrid energy systems and adaptive energy management for hybrid electric vehicles. *Energy Convers. Manag.* **2021**, *243*, 114357. [[CrossRef](#)]
23. Abo-elyousr, F.K.; Nozhy, A.N. Bi-objective Economic Feasibility of Hybrid Micro- Grid Systems with Multiple Fuel Options for Islanded Areas in Egypt. *Renew Energy* **2018**, *128*, 37–56. [[CrossRef](#)]
24. Hou, S.; Gao, J.; Zhang, Y.; Chen, M.; Shi, J.; Chen, H. A comparison study of battery size optimization and an energy management strategy for FCHEVs based on dynamic programming and convex programming. *Int. J. Hydrogen Energy* **2020**, *45*, 21858–21872. [[CrossRef](#)]
25. Gautham Prasad, G.; Shetty, N.; Thakur, S.; Rakshitha Bommegowda, K.B. Supercapacitor technology and its applications: A review. *IOP Conf. Ser. Mater. Sci. Eng.* **2019**, *561*, 012105. [[CrossRef](#)]
26. Borhanazad, H.; Mekhilef, S.; Gounder Ganapathy, V.; Modiri-Delshad, M.; Mirtaheri, A. Optimization of micro-grid system using MOPSO. *Renew. Energy* **2014**, *71*, 295–306. [[CrossRef](#)]

Disclaimer/Publisher's Note: The statements, opinions and data contained in all publications are solely those of the individual author(s) and contributor(s) and not of MDPI and/or the editor(s). MDPI and/or the editor(s) disclaim responsibility for any injury to people or property resulting from any ideas, methods, instructions or products referred to in the content.